Describing the properties of compressed expanded graphite through power laws

2003 J. Phys.: Condens. Matter 15 7213

(http://iopscience.iop.org/0953-8984/15/43/006)

INSTITUTE OF PHYSICS PUBLISHING JOURNAL OF PHYSICS: CONDENSED MATTER

J. Phys.: Condens. Matter **15** (2003) 7213–7226 PII: S0953-8984(03)67656-3

Describing the properties of compressed expanded graphite through power laws

A Celzard[1], **J F Marêché and G Furdin**

Laboratoire de Chimie du Solide Minéral, Université Henri Poincaré—Nancy I, UMR-CNRS 7555, BP 239, 54506 Vandoeuvre-lès-Nancy, France

E-mail: Alain.Celzard@lcsm.uhp-nancy.fr

Received 18 August 2003
Published 17 October 2003
Online at stacks.iop.org/JPhysCM/15/7213

Abstract

In this paper, valuable formulae describing the behaviour of a number of physical properties of moderately compressed expanded graphite (CEG) are given. Many of these relationships provide confirmations of empirical power law equations which had remained unexplained. Other physical properties are also described for the first time with power laws whose exponents are derived rigorously. On the basis of early works by the authors, the origins of the observed behaviours are explained, hence providing a better understanding of the material. Thus, the variations with the density of CEG of the thermal and electrical conductivities, elastic moduli, mosaicities, permeabilities, formation factors, characteristic pore radii and diameters, surface areas and open pore volumes are described. Power laws are shown to apply, and the values of the corresponding exponents are compared both with the results of the authors and with those from the literature.

1. Introduction

In the past few years, many experimental and theoretical works have been performed on compressed expanded graphite (CEG). The latter is a self-consolidated material readily prepared by unidirectional compaction of raw exfoliated graphite, which comprises tortuous and highly deformable worm-like particles. The interlocking of such worms leads to highly porous materials, whose properties are worth studying as a function of density. Due to the numerous applications of expanded graphite, ranging from energy storage to catalysis, heavy oil abatement and even in biology, a suitable modelling is required. Observing the variations of a number of physical properties while the material is increasingly compressed, several authors have suggested some empirical laws, which may be summarized as $\Psi \propto d^{\pm\alpha}$; Ψ is the property under study, d is the density of the material, and α is an exponent. Such relationships were

[1] Author to whom any correspondence should be addressed.

found to apply to many different physical quantities, but had not been explained. Moreover, most of the values derived for the exponent α were neither explained nor related to any rigorous model. In the present paper, all the physical properties of CEG measured so far are gathered together and examined; the above power laws are now rigorously derived, while several others, rigorous or not, are given. It will be shown that these power laws are just the limiting forms for $d \to 0$ of more accurate equations already established by the present authors.

Several necessary concepts dealing with CEG are first recalled in section 2. The physical properties of the graphite backbone and those of the pore space are then detailed in sections 3 and 4, respectively. For each property it is shown that, in agreement with what was empirically found by a number of authors, power laws may be derived. The corresponding exponents, rigorous or not, depending on the cases, are discussed and compared with what was obtained from various research papers.

2. Materials

2.1. Preparation of CEG samples

CEG samples were prepared by axial compaction of raw EG worms in a square tube. Compressing them obviously induces some orientation in the material, in such a way that every graphite sheet tends to lie within a plane perpendicular to the pressing stress. Anisotropic properties are thus expected—hence the chosen geometry for the samples, for which two directions of measurement are defined. Just like in monocrystalline graphite, the direction *a* corresponds to the bedding plane of the graphite flakes, i.e., is perpendicular to the applied pressure, while *c* is the orthogonal direction. At the beginning of the compaction, the worms first rearrange spatially, then interlock with each other as soon as the rigidity threshold of the system is reached, and finally deform and collapse when the compression proceeds further [1]. Materials having the lowest densities, typically below 0.05 g cm^{-3}, are still isotropic, but more compressed samples become increasingly anisotropic as the density rises (see further on in the text).

Except for investigating those properties for which no anisotropy is expected (surface area, open pore volume, mosaicity), all the samples prepared by the present authors were cubes with sides of 2 cm. Other experimental data cited and used in this work were obtained from similar samples, possibly parallelepipedic or even cylindrical in some cases, or with slightly different sizes. However, the above definition of directions *a* and *c* remains the same and applies to any sample.

2.2. Varieties of EG

The results of the present authors were obtained from two distinct batches of EG, termed EG_1 and EG_2 in the following, both supplied by the French company Le Carbone-Lorraine. Their main features have already been extensively detailed (see for example [2, 3]), but should be briefly recalled here. The worms have the same expansion factor and the same density in the two materials, but exhibit different aspect ratios (length/diameter), thus leading to different apparent densities for the raw uncompacted EG, i.e., 7.5×10^{-3} and 2.6×10^{-3} g cm^{-3} for EG_1 and EG_2, respectively. Besides this, the typical graphite flakes within the worms of each material do not have the same dimensions, those of EG_2 being thinner and larger than those of EG_1 (thickness 15 and 23 nm, diameter 32 and 13 μm, respectively).

The other materials whose properties were described in the literature and are reported here have various apparent densities in the uncompacted state, ranging from 1.7×10^{-3} to

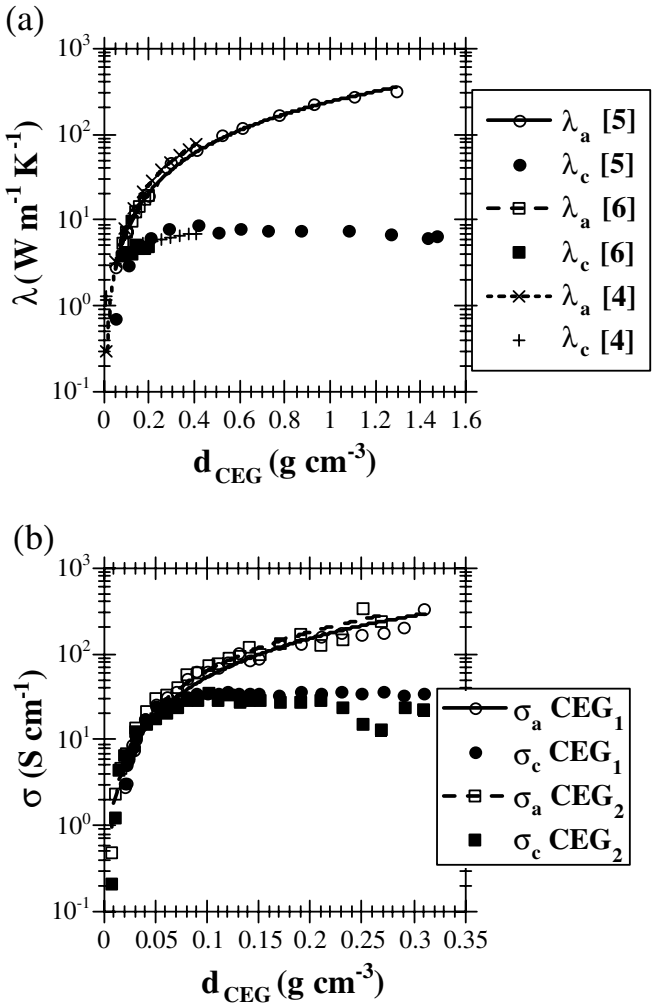

Figure 1. (a) Thermal conductivities (λ) of various blocks of CEG taken from the literature (references are given in brackets). The curves are power laws fitted to the values measured along the direction a, with exponents close to 1.5 (see the text), thus supporting equation (1). (b) The same as (a) but for electrical conductivities (σ); the samples are from the authors ($CEG_{1,2}$), and equation (3) is checked with values measured along a.

12×10^{-3} g cm^{-3}. Some of them also originate from Le Carbone-Lorraine. It will be seen below that such initial differences influence the absolute values of the physical properties, but do not change their quantitative behaviour when the density, d, is increased.

3. Physical properties of the graphite backbone

3.1. Thermal and electrical conductivities

The thermal conductivities λ were measured in both directions a and c for several varieties of CEG [4–6]. The data points shown in figure 1(a) could be fitted by power laws with exponents equal to 1.45 (direction a) and 0.27 (direction c) [6], and 1.50 (direction a) and 0.43 (direction c)

[4, 5]. λ_a and λ_c thus vary in very different ways over a wide range of d; however, $\lambda_a \approx \lambda_c$ at low densities. It may be seen from the experimental data that, as $d \to 0$, the following single relationship applies, whatever the direction of measurement:

$$\lambda \propto d^{1.5}. \tag{1}$$

Indeed, it seems that the exponent which holds at low densities is that corresponding to direction a only, and this was also observed for both electrical conductivity and elastic modulus (see below). This finding probably originates from the intrinsically anisotropic properties of graphite: their lower values along the direction c of the individual graphite sheets combined with the orientation should indeed hinder the increases of these properties when the density is increased.

Equation (1) may be justified by percolation theory. If the graphite is supposed to be heat conducting while the pore phase is not, then the EG is non-conducting as long as a conductivity threshold d_c is not reached. For conductivity problems, d_c corresponds to the connectivity threshold, which is slightly lower than the apparent density of the raw uncompacted EG [7]. Above d_c, percolation theory predicts that the thermal conductivity obeys

$$\lambda \propto (d - d_c)^t, \tag{2}$$

where t is a critical exponent close to 2 for any classical three-dimensional system [8]. Whatever the variety of expanded graphite, d_c is much lower than the usual values of the densities of CEG blocks. Thus, equation (1) experimentally observed by several authors [4–6] is just an approximation of equation (2) for small d_c. Moreover, equating (1) with (2) explains why the exponent of the former power law is slightly smaller than t.

The same reasoning strictly applies to the case of the electrical conductivity, since it was shown [3, 7] that equation (2) works with the same conductivity threshold d_c and the same exponent t. Consequently, the simple following power law is expected to describe correctly the electrical conductivity σ, at least along the direction a, for wide ranges of density, and along both directions for $d \to 0$:

$$\sigma \propto d^{1.5}. \tag{3}$$

Figure 1(b) shows the application of (3) to the experimental electrical conductivities measured along direction a for CEG_1 and CEG_2 blocks. Exponents equal to 1.50 and 1.49, respectively, are obtained. Finally, it should be noted that equation (1) was found empirically to work for both silica [9] and carbon [10] aerogels, while (3) was recovered for monolithic carbon aerogels [10].

3.2. Elastic moduli

The elastic modulus E of highly porous materials, such as silica aerogels, may be described by the following relationship over wide ranges of density [11–13]:

$$E \propto d^{\gamma}. \tag{4}$$

In (4), γ is an exponent whose expected value, based on bending deformation of microstructural beams, is close to 2 [11]. However, higher values of γ (up to 4) were already reported, and microstructural models were suggested accordingly [12, 13].

As regards CEG, elastic percolation was already invoked to account for the observed behaviours of elastic moduli E_a and E_c measured in directions a and c, respectively [3, 14]. E is zero below the rigidity threshold, d_r, and above such a critical density, E reads

$$E \propto (d - d_r)^f, \tag{5}$$

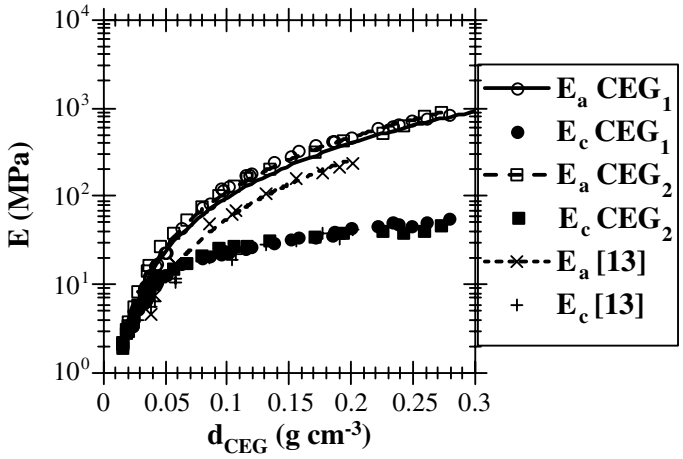

Figure 2. Elastic moduli (E) as a function of density; the data are from the authors (CEG$_{1,2}$), and from the reference given in brackets. The curves are power laws fitted to the values measured along the direction a, with exponents close to 2 (see the text), thus supporting equation (6).

where f is a critical exponent whose value depends on the kind of elastic force within the material. In three-dimensional systems, it was shown that central forces (i.e., normal to the particle surfaces) are predominant when $f \approx 2$, while f is found to be close to 4 when bond-bending forces or beams describe better the micromechanical characteristics (see [3, 14] and references therein). In the case of CEG, the values of d_r, though higher than those of d_c, are still low, and hence equation (5) may be approximated by

$$E \propto d^2. \tag{6}$$

In (6), the exponent is a little higher than in both (1) and (3) because, for any given value of d, $(d - d_r) < (d - d_c)$. Figure 2 shows that (6) is well obeyed, with exponents of 2.05 (CEG$_1$), 2.05 (CEG$_2$), and 2.23 (data from [15]), at least for E_a, over a wide range of d, and for E_c for $d \to 0$. These features are thus similar to what was found for both thermal and electrical conductivities.

3.3. Mosaicity

In a previous work [1], the excluded volume of thin discs was calculated and used to show that, while EG worms are undergoing compaction, the angle of greatest disorientation β of the graphite sheets within the worms obeys the following equation:

$$2\beta - \sin(2\beta) = \frac{\text{density of graphite}}{d_{\text{worm}}} \times \frac{2}{\text{aspect ratio of the graphite sheets}}. \tag{7}$$

In equation (7), the density of graphite is assumed to be 2.2 g cm^{-3}, and the aspect ratio of the graphite sheets is the diameter to thickness ratio of the constitutive graphite discs within the worms. For both CEG$_1$ and CEG$_2$, such an average thickness was deduced from surface area measurements of the raw uncompacted material, while the diameter was calculated from aspect ratios derived from application of effective-medium theory to the conductivity data of CEG blocks [7].

To second order in β, (7) becomes

$$2\beta - 2\beta + \frac{(2\beta)^3}{6} \propto d_{\text{worm}}^{-1}. \tag{8}$$

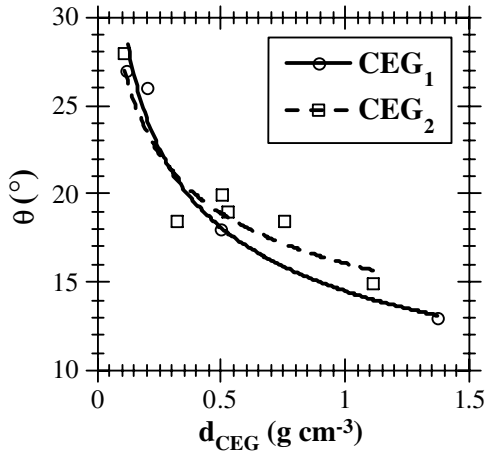

Figure 3. The mean angle of disorientation (θ) (i.e., mosaic spread) of the graphite sheets within CEG_1 and CEG_2 blocks. The curves are power laws with exponents close to $-1/3$ (see the text), thus supporting equation (12).

The density of the worms within the CEG blocks was calculated according to

$$d_{\text{worm}} = \frac{d}{1 - \kappa\left(1 - \frac{d}{\text{density of graphite}}\right)}, \tag{9}$$

where κ is a constant derived from the rigidity threshold of each EG [1]. For $d \to 0$, the limiting form of equation (9) is

$$d_{\text{worm}} \propto d. \tag{10}$$

Substituting (10) in (8) leads to

$$\beta \propto d^{-1/3}. \tag{11}$$

Now the mosaic spread, which corresponds to the average disorientation angle θ between the graphite sheets in the whole CEG, is directly proportional to β [1], and hence

$$\theta \propto d^{-1/3}. \tag{12}$$

Equation (12) may be checked for both sets of mosaicity results, corresponding to CEG_1 and CEG_2, obtained from XRD measurements. Figure 3 thus shows the mosaic spread for both materials. Fitting a power law to the experimental points leads to exponents equal to -0.32 and -0.23, respectively, i.e., close to $-1/3$.

4. Physical properties of the pore space

The following now deals with a number of properties describing the pore space of CEG blocks, namely permeability, formation factor, hydraulic and dynamically interconnected pore radii, and critical pore diameter. Before detailing each of these properties, a few definitions should first be recalled.

The permeability, k, has the dimension of an area, and hence it may be seen as representing the cross-section of an effective channel for fluid flow through the pore space. k is thus proportional to a squared length L_0 such that [16]

$$k = \frac{L_0^2}{F}, \tag{13}$$

where F is the so-called formation factor. F is an adimensional parameter defined for materials whose pore space may be saturated with a conducting fluid, such as brine. It is simply the ratio of the conductivities of the free electrolyte (χ_0) to that of the saturated pore phase of the material under study (χ). F is related to both the tortuosity factor τ and to the open porosity P according to $F = \tau/P$. Unlike k, the parameters F and τ are scale-invariant quantities, meaning that if the sizes of the pores and those of the solid grains are magnified or shrunk, leaving the porosity unchanged, their values are unaffected. Equation (13) is thus a convenient formula since it both expresses that k has the dimension of an area and includes the tortuosity and the volume fraction of voids through F.

Depending on the theories, L_0 may take several meanings; hence the various definitions below.

4.1. Characteristic pore radii and diameters

According to the authors of several major research papers and reviews dealing with the description of porous media [16–21], the characteristic pore radius (or diameter) may have different definitions. The older theory of Carman and Kozeny deals with the so-called hydraulic radius r_h defined as

$$r_h = \frac{2V_p}{S_p}, \tag{14}$$

where V_p and S_p are the volume and the surface of the pore space, respectively [18, 19].

An alternative pore radius, Λ, was proposed by Johnson *et al* [20], and corresponds to a 'dynamically connected pore size'. It may be derived from measurements of the electrical conductivity of the electrolyte-saturated pore phase, and reads

$$\Lambda = 2\frac{\int |\nabla\zeta(r)|^2 \, \mathrm{d}V_p}{\int |\nabla\zeta(r)|^2 \, \mathrm{d}S_p} = 2\frac{V_p}{mS_p}, \tag{15}$$

where $\nabla\zeta(r)$ is the potential drop across the pore of radius r, and m is a constant found experimentally to be close to 1.5. For ideal porous media made of a packing of spherical grains, Λ was shown to obey the following equation [20]:

$$\Lambda = \frac{2PD}{9(1-P)}, \tag{16}$$

where D is the grain diameter. Describing CEG as a packing of porous graphite spheres is indeed a very rough model; nevertheless the latter was shown to work correctly in the density range of interest, i.e., for $0 < d < 0.3$ g cm^{-3} [22]. Since, for a spherical grain,

$$D = \sqrt[3]{\frac{6M}{\pi d_{worm}}} \propto d_{worm}^{-1/3}, \tag{17}$$

where M is the mass of the grain, substituting (17) and (10) in (16), one gets

$$\Lambda \propto d^{-4/3}. \tag{18}$$

Thus, the values of Λ, already presented in a previous paper dealing with CEG_1 [22], may be fitted by a power law such that the exponent is indeed -1.37. However, since Λ was calculated from equations (16) to (17), it is obvious that one will find such an exponent to be close to $-4/3$. Consequently the following, which consists in checking (18) from separate data, is worth developing.

The parameter δ_c introduced by Katz and Thompson [21, 23] is one more possible definition for the characteristic pore size. It may be obtained from intrusion experiments of a

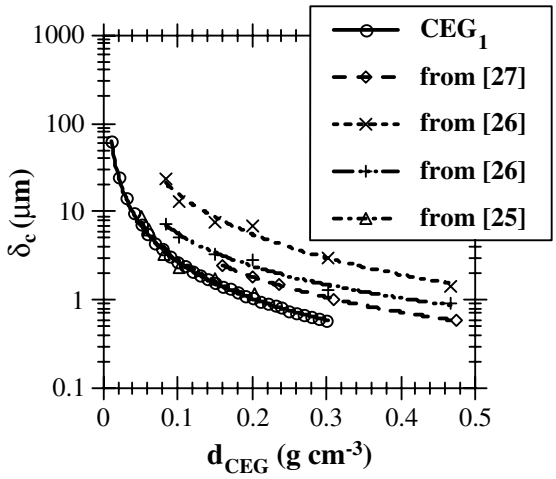

Figure 4. Critical pore diameters (δ_c) derived from intrusion porosimetry experiments. The data are from the authors (CEG_1) and from the references given in the brackets. The curves are power laws with exponents close to $-4/3$ (see the text), thus supporting equation (21).

fluid—usually mercury—and corresponds to the critical pore diameter at which the invading fluid first forms a connected path spanning the sample. δ_c is located at the inflection point of the experimental injection curve, i.e., it is the abscissa of the maximum of the plot of incremental intruded volume versus pore diameter. Since, for a given porous medium, the product permeability $k \times$ formation factor F is such that [16, 24]

$$\begin{aligned} kF &\propto \Lambda^2, \\ kF &\propto \delta_c^2; \end{aligned} \tag{19}$$

thus

$$\delta_c \propto \Lambda, \tag{20}$$

and hence, given (18),

$$\delta_c \propto d^{-4/3}. \tag{21}$$

A number of mercury porosimetry measurements were performed on CEG, from which the curves for δ_c versus d were built up. As shown in figure 4, fitting a power law to the experimental results of [25] gives the exponent -1.75, while the data points of [26] lead to -1.34 and -1.66, and those of [27] to -1.34. Finally, the data of [4] lead to an exponent of -1.4. All these values are indeed close to $-4/3$, thus supporting equation (21) but also equation (18) through (20).

Coming back to the hydraulic radius introduced above (equation (14)), r_h was calculated for CEG_1 blocks from open pore volumes (measured by helium pycnometry) and from surface areas (measured by krypton adsorption at 77 K). The results are shown in figure 5 and, again, a power law may be fitted to the data points; one finds

$$r_h \propto d^{-0.94}. \tag{22}$$

Understanding such an exponent, close to -1, is not so easy. Indeed, Kozeny–Carman theory states that

$$k = \frac{(V_p/S_p)^2}{2F} = \frac{r_h^2}{8F}. \tag{23}$$

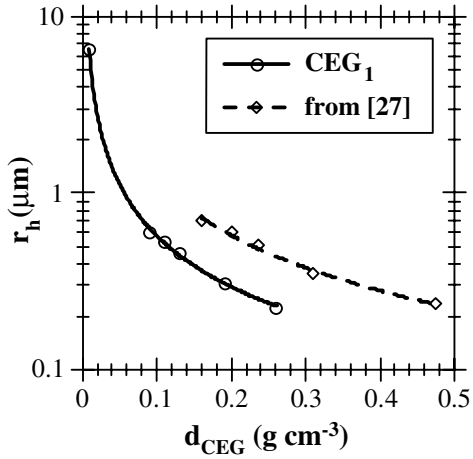

Figure 5. Hydraulic radii as a function of density for CEG_1 and for samples from the reference given in brackets. The curves are power laws with exponents close to -1 (see the text), thus supporting equation (22).

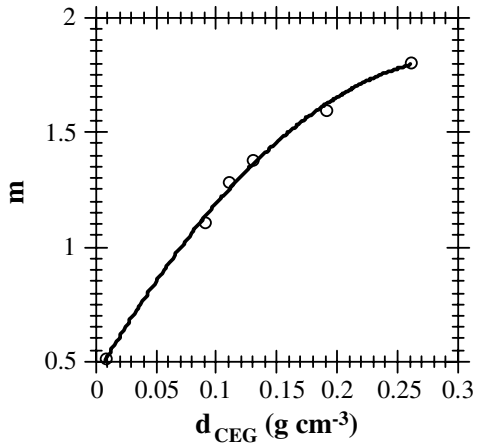

Figure 6. The parameter m of equation (15), showing that m is not a constant but depends on the density. However, m is still close to 1.5 in the relevant porosity range. The curve is just a guide for the eye.

Hence, combining (23) and (19), one gets:

$$kF \propto r_h^2 \propto \Lambda^2 \propto \delta_c^2. \tag{24}$$

Consequently, the theoretical value of the exponent in equation(22) would be that of both Λ and δ_c, i.e., $-4/3$. Thus, the experimental uncertainties in the measurements of both V_p and S_p could account for the deviation observed in the value of the exponent.

Otherwise, the observed variation of r_h as a function of d is really slightly different from that of the other pore sizes Λ and δ_c. This latter interpretation is justified by the fact that a very similar power law, $r_h \propto d^{-1.04}$, was obtained elsewhere [27] (see figure 5), and could also explain why the agreement observed between the calculated values of Λ from equations (16) to (17), on the one hand, and from equation (15), on the other hand, is correct, but not very accurate [28]. In such conditions, the parameter m within equation (15) should depend on d. Plotting m calculated from (15) and from the experimental values of V_p and S_p does indeed show—see figure 6—that this parameter is not a constant, even if its value is close to 1.5 in the relevant range of density.

4.2. Permeability and formation factor

It is well known that the effective conductivity χ of porous media saturated with a conducting fluid follows the so-called Archie law [29], later explained on the basis of percolation theory [30]. It reads

$$\chi = \chi_0 P^n, \tag{25}$$

where χ_0 is the conductivity of the saturating fluid and n is an empirical exponent referred to as the 'cementation index' [31]. Besides this, the permeability k is often described over wide porosity ranges according to an old empirical relationship ([18, 19, 32] and references therein), later confirmed by effective-medium theory [18]:

$$k \propto P^{n'}. \tag{26}$$

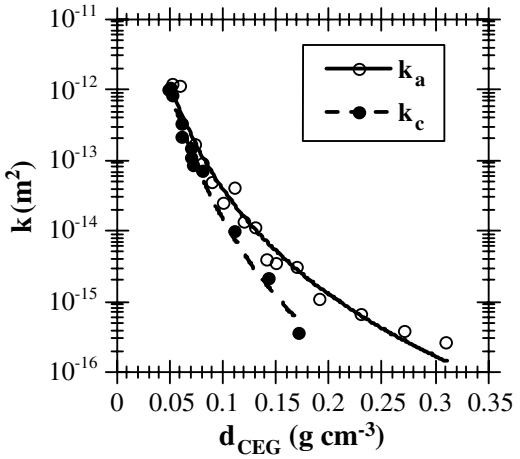

Figure 7. Permeabilities (k) of CEG_1 blocks, measured along a and c directions. The curves are power laws with exponents close to $-16/3$ (see the text), thus supporting equation (30).

In (26), n' is another empirical exponent related to n by the following relationship, which was confirmed by many experimental studies [33]:

$$n' = 2n. \tag{27}$$

Since $F = \chi_0/\chi$, combining (25), (26), and (27), one gets

$$k \propto F^{-2}. \tag{28}$$

Equation (28) was already checked elsewhere with permeabilities and formation factors of CEG_1 blocks [28], and may be used now for deriving the variation of both k and F versus the density d of the material. Indeed, substituting (28) in (19) leads to

$$\begin{aligned} &k \propto \Lambda^4, \delta_c^4, \\ &F \propto \Lambda^{-2}, \delta_c^{-2}. \end{aligned} \tag{29}$$

By virtue of equations (18) and (21), one finally gets

$$k \propto d^{-16/3} \tag{30}$$

and

$$F \propto d^{8/3}. \tag{31}$$

As shown in figure 7, equation (30) is correct according to the experimental data of the present authors (CEG_1 blocks), leading to exponents equal to -4.93 and -6.11 for permeabilities measured in the directions a and c, respectively. Other works performed on samples of the same kind lead to exponents of -4.71 (direction a) and -5.06 (direction c) [25], -5 (direction a) and -6 (direction c) [26], and -5.03 (direction c) [5]. All these data are in good agreement with the expected value of $-16/3$.

Much less work was devoted to the experimental determination of the formation factors. Anyway, the anisotropy seems to induce severe deviations from equation (31) since only one single set of data is in agreement with the latter. Indeed, fitting a power law to the values of F measured by the present authors on CEG_1 blocks leads to exponents of 1.29 (direction a) and 1.65 (direction c) [22]. It is rather surprising that these exponents are so different from $8/3$, since the measured F were shown to be in agreement with the calculated ones, for

which exponents of 2.15 (direction a) and 3.38 (direction c) may be derived [22]. In another work [26], the formation factors were described by exponential laws. Fitting a power law to these data leads to exponents equal to 0.97 (direction a) and $2.70 \approx 8/3$ (direction c). It thus seems that only the formation factors measured along the direction c could be described by equation (31), similar to what was observed for λ_a, σ_a, and E_a with their respective power laws.

4.3. Surface area and open pore volume

The modelling of a system of accordions undergoing compaction was performed recently, and the surface area was calculated accordingly [2]. Good agreements were found between measured and calculated areas for both varieties CEG_1 and CEG_2. In this previous study, the same concepts as those dealing with the mosaicity were used, thus supporting the former modelling of the compaction of EG [1]. It was shown that, despite the simplicity of the geometrical model invoked, the surface area S_p is a very complex function of the angles between graphite flakes, their aspect ratios, and the density of the CEG blocks, all these quantities being linked with each other. However, when $d \to 0$, and to first order in d, S_p can be written as

$$S_p \approx x + yd^{-1/2}, \tag{32}$$

where x and y are constants. In the present work, the physical properties of CEG are described by power laws, and thus it is useful to rewrite equation (32) in the form

$$S_p \approx zd^{-q}. \tag{33}$$

Equating (32) with (33) for $d \to 0$ gives the following relationship:

$$q \approx \frac{\ln(z/x) - (y/x)d^{-1/2}}{\ln d}. \tag{34}$$

In the usual range of density within which most of the measurements on CEG blocks were made, i.e., for $0.01 < d < 0.3$ g cm^{-3}, the exponent q is close to 0.13 for both CEG_1 and CEG_2. Moreover, the surface area derived from an electrochemical method for other CEG samples [27] may also be fitted by a power law with an exponent -0.16. The surface area of moderately compressed EG may thus be described by $S_p \propto d^{-0.13}$ but, unlike the previous exponents, $q = 0.13$ is not rigorous since it is density dependent (see equation (34)). However, such an approximation is not so bad, as seen in figure 8, and may be useful for describing the behaviour of the open pore volume V_p.

Indeed, given equations (14), (22), and (33), V_p is expected to vary as

$$V_p \propto d^{-1.1}. \tag{35}$$

Incidentally, if $r_h \propto \Lambda \propto d^{-4/3}$ is correct, then

$$V_p \propto d^{-1.46} \sim d^{-3/2}. \tag{36}$$

Figure 9 exhibits the specific pore volume, obtained from helium pycnometry measurements performed on CEG_1, plotted as a function of the density. The power law fitted to the data points gives an exponent of -1.04, thus supporting equation (35) rather than (36).

Finally, the open porosity may be calculated from

$$P = V_p d \tag{37}$$

and hence, substituting (35) in (37),

$$P \propto d^{-0.1}. \tag{38}$$

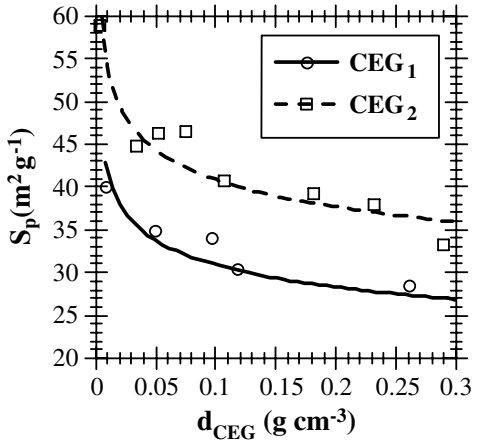

Figure 8. Specific surface areas (S_p) of CEG_1 and CEG_2 blocks. The curves are power laws with exponents close to −0.13 (see the text), thus supporting equation (33) and hence (32) through (34).

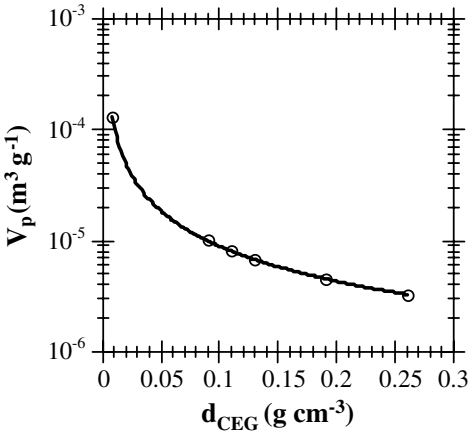

Figure 9. Specific pore volumes (V_p) of CEG_1. The curve is a power law with an exponent close to −1.1 (see the text), thus supporting equation (35).

Such a result seems to be in contradiction with other works for which the open porosity is a linear decreasing function of d [26, 27]. However, it should be noticed that equation (38) may be rewritten as $P \propto [d_0 + (d - d_0)]^{-0.1}$, where $d_0 \gg 0$ is a given value of the density. Taylor expansion to first order in d thus leads to

$$P \sim a - bd \qquad \text{with} \begin{cases} a = 1.1 d_0^{-0.1} \\ b = 0.1 d_0^{-1.1}. \end{cases} \tag{39}$$

Thus, the data points for P versus d may also be fitted by a straight line, and even more satisfactorily the exponent within equation (38) is very small, which is actually the case here. Figure 10 does indeed show that the results of the present authors may be described by a linear law; incidentally, the data points are very similar to those of [26]. Such a way of rewriting power laws in d dealing with small exponents through Taylor expansion also explains why, in a given range of density, the surface area may be seen as linearly decreasing with d [27] (while a power law is evidenced as soon as a wider range of density is studied). Moreover, the mosaic spread for which the exponent is rather small ($-1/3$) could also be seen as linearly decreasing within the range of d studied (see figure 3).

5. Conclusions

On the basis of early works and supported by a number of data from the literature, many useful power law equations describing the physical properties of CEG were proposed. Most of them apply over the whole range of densities $0 < d < 0.3$ g cm^{-3}, whatever the direction of measurement. However, due to the sometimes strong anisotropies, a few of these power laws apply only along one single direction, either a or c. In such a case, the properties concerned along the other direction are described by the same equations in a vanishingly small range of d when $d \to 0$. All of these power laws are listed in table 1.

In table 1, the fractional exponents are rigorous, while the others are not, either because no analytical expression is available yet (e.g. r_h, V_p) or because the power law is just an estimate of a more accurate equation (e.g. λ, σ, E, S_p). However, such simple equations allow one to predict how many physical properties vary when expanded graphite is compressed.

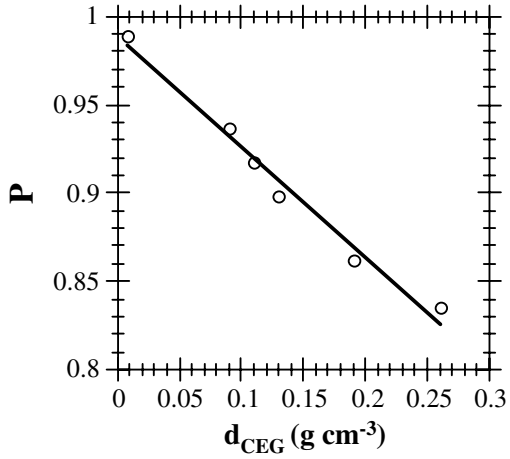

Figure 10. Open porosity (P) of CEG_1. Just like in other works, the data may be described by a straight line.

Table 1. Power laws describing the physical properties of CEG blocks as a function of their density d.

Properties of CEG described by power laws			
Graphite backbone		Pore space	
Thermal conductivity	$\lambda_a \propto d^{1.5}$	Dynamic pore radius	$\Lambda \propto d^{-4/3}$
Electrical conductivity	$\sigma_a \propto d^{1.5}$	Critical pore diameter	$\delta_c \propto d^{-4/3}$
Elastic modulus	$E_a \propto d^2$	Hydraulic radius	$r_h \propto d^{-0.94}$
Mosaic spread	$\theta \propto d^{-1/3}$	Permeability	$k \propto d^{-16/3}$
		Formation factor	$F_c \propto d^{8/3}$
		Surface area	$S_p \propto d^{-0.13}$
		Open pore volume	$V_p \propto d^{-1.1}$

Acknowledgments

The authors would like to thank the CNRS (DSC and DRI) for financial support through the GDRE 'Matériaux carbonés et environnement' and the France–Poland twinning 'Matériaux carbonés et catalytiques pour l'environnement'. This work was also partially supported by the ADEME agency, by the MAE and by the 'Conseil Général de Lorraine'.

References

[1] Celzard A, Schneider S and Marêché J F 2002 *Carbon* **40** 2185
[2] Celzard A, Marêché J F and Furdin G 2002 *Carbon* **40** 2713
[3] Celzard A, Krzesiñska M, Marêché J F and Puricelli S 2001 *Physica* A **294** 283
[4] Py X, Olives R and Mauran S 2001 *Int. J. Heat Mass Transfer* **44** 2727
[5] Bonnissel M, Luo L and Tondeur D 2001 *Carbon* **39** 2151
[6] Olives R and Mauran S 2001 *Transport Porous Media* **43** 377
[7] Celzard A, Marêché J F, Furdin G and Puricelli S 2000 *J. Phys. D: Appl. Phys.* **33** 3094
[8] Sahimi M 1994 *Applications of Percolation Theory* (Bristol, PA: Taylor and Francis)
[9] Fricke J, Lu X, Wang P, Büttner D and Heinemann U 1992 *Int. J. Heat Mass Transfer* **35** 2305
[10] Lu X, Nilsson O, Fricke J and Pekala R W 1993 *J. Appl. Phys.* **73** 581

[11] Gross J, Schlief T and Fricke J 1993 *Mater. Sci. Eng.* A **168** 235
[12] Emmerling A, Gross J, Gerlach R, Goswin R, Reichenauer G, Fricke J and Haubold H G 1990 *J. Non-Cryst. Solids* **125** 230
[13] Gross J and Fricke J 1995 *Nanostruct. Mater.* **6** 905
[14] Krzesińska M, Celzard A, Marêché J F and Puricelli S 2001 *J. Mater. Res.* **16** 606
[15] Krzesińska M 1999 *Acoust. Lett.* **23** 39
[16] Le Doussal P 1989 *Phys. Rev.* B **39** 4816
[17] Schwartz L M, Martys N, Benz D P, Garboczi E J and Torquato S 1993 *Phys. Rev.* E **48** 4584
[18] Sahimi M 1995 *Flow and Transport in Porous Media and Fractured Rocks* (Weinheim: VCH)
[19] Dullien F A L 1979 *Porous Media—Fluid Transport and Pore Structure* (New York: Academic)
[20] Johnson D L, Koplik J and Schwartz L M 1986 *Phys. Rev. Lett.* **57** 2564
[21] Katz A J and Thompson A H 1986 *Phys. Rev.* B **34** 8179
[22] Celzard A and Marêché J F 2002 *J. Phys.: Condens. Matter* **14** 1119
[23] Katz A J and Thompson A H 1987 *J. Geophys. Res.* **92** 599
[24] Banavar J R and Johnson D L 1987 *Phys. Rev.* B **35** 7283
[25] Biloé S and Mauran S 2003 *Carbon* **41** 525
[26] Mauran S, Rigaud L and Coudevylle O 2001 *Transport Porous Media* **43** 355
[27] Calas-Blanchard C, Comtat M, Marty J L and Mauran S 2003 *Carbon* **41** 123
[28] Celzard A, Marêché J F and Perrin A 2002 *Fuel Process. Technol.* **77/78** 467
[29] Archie G E 1942 *Trans. AIME* **146** 54
[30] Balberg I 1986 *Phys. Rev.* B **33** 3618
[31] Sen P N, Scala C and Cohen M H 1981 *Geophysics* **46** 781
[32] Scheidegger A E 1974 *The Physics of Flow through Porous Media* 3rd edn (Toronto: University of Toronto Press)
[33] Wong P, Koplik J and Tomanic J P 1984 *Phys. Rev.* B **30** 6606